Bone. Author manuscript; available in PMC: 2020 Aug 1.
Published in final edited form as: Bone. 2019 May 20;125:160–168. doi: 10.1016/j.bone.2019.05.024

The $Ca_V1.2$ L-type calcium channel regulates bone homeostasis in the middle and inner ear

Chike Cao [a,*], Aaron B Oswald [b], Brian A Fabella [b], Yinshi Ren [c,d], Ramona Rodriguiz [e], George Trainor [f], Matthew B Greenblatt [g,h], Matthew J Hilton [c,d], Geoffrey S Pitt [a]

Author information Article notes Copyright and License information

PMCID: PMC6615562 NIHMSID: NIHMS1531213 PMID: 31121355

Abstract

Bone remodeling of the auditory ossicles and the otic capsule is highly restricted and tightly controlled by the osteoprotegerin (OPG) / receptor activator of nuclear factor kappa-B ligand (RANKL) / receptor activator of nuclear factor kappa-B (RANK) system. In these bony structures, a pathological decrease in OPG expression stimulates osteoclast differentiation and excessive resorption followed by accrual of sclerotic bone, ultimately resulting in the development of otosclerosis, a leading cause of deafness in adults. Understanding the signaling pathways involved in maintaining OPG expression in the ear would shed light on the pathophysiology of otosclerosis and other ear bone-related diseases. We and others previously demonstrated that Ca^{2+} signaling through the L-type $Ca_V1.2$ Ca^{2+} channel positively regulates OPG expression and secretion in long bone osteoblasts and their precursor cells *in vitro* and *in vivo*. Whether $Ca_V1.2$ regulates OPG expression in ear bones has not been investigated. We drove expression of a gain-of-

function $Ca_V1.2$ mutant channel ($Ca_V1.2^{TS}$) using *Col2a1-Cre,* which we found to target osteochondral/osteoblast progenitors in the auditory ossicles and the otic capsule. *Col2a1-Cre;*$Ca_V1.2^{TS}$ mice displayed osteopetrosis of these bones shown by μCT 3D reconstruction, histological analysis, and lack of bone sculpting, findings similar to phenotypes seen in mice with an osteoclast defect. Consistent with those observations, we found that *Col2a1-Cre;*$Ca_V1.2^{TS}$ mutant mice showed reduced osteoclasts in the otic capsule, upregulated mRNA expression of *Opg* and *Opg/Rankl* ratio, and increased mRNA expression of osteoblast differentiation marker genes in the otic capsule, suggesting both an anti-catabolic and anabolic effect of $Ca_V1.2^{TS}$ mutant channel contributed to the observed morphological changes of the ear bones. Further, we found that *Col2a1-Cre;*$Ca_V1.2^{TS}$ mice experienced hearing loss and displayed defects of body balance in behavior tests, confirming that the $Ca_V1.2$-dependent Ca^{2+} influx affects bone structure in the ear and consequent hearing and vestibular functions. Together, these data support our hypothesis that Ca^{2+} influx through $Ca_V1.2^{TS}$ promotes OPG expression from osteoblasts, thereby affecting bone modeling/remodeling in the auditory ossicles and the otic capsule. These data provide insight into potential pathological mechanisms underlying perturbed OPG expression and otosclerosis.

Keywords: $Ca_V1.2$, Ca^{2+} signaling, osteoprotegerin, otosclerosis, osteoclast

1. Introduction

The middle ear contains the three auditory ossicles—the malleus, incus, and stapes—which sequentially conduct sound by transmitting sound vibrations from the tympanic membrane to the fluid in the cochlea via the oval window of the otic capsule, the bony case enclosing the cochlea and vestibular system. In the otic capsule, the vibrations are converted into electrical signals and transduced to the brain via auditory nerves [1]. Abnormal morphological changes of the bone structures in the auditory ossicles or the otic capsule may disturb sound transmission and cause conductive hearing loss and/or vestibular dysfunction.

The auditory ossicles and the otic capsule, unlike most bones in the skull that form through intramembranous ossification, develop like long bones through endochondral ossification. In this process an initial cartilage template is subsequently replaced by bone while the terminally differentiated hypertrophic chondrocytes and the calcified cartilage matrix are removed by osteoclasts (bone modeling phase) [2, 3]. Absence of osteoclastic bone resorption in mice with osteoclast defects results in osteopetrotic phenotype of these bones, significantly affecting their morphology and function [4]. However, unlike long bones, no significant bone remodeling (a coupled process of osteoclastic bone resorption with subsequent osteoblastic formation) occurs in the auditory ossicles or the otic capsule after development [5]. Turnover of the otic capsule in regions surrounding the perilymph spaces is about 0.13% per year compared to 10% for the long bones [6]. This low bone remodeling rate in the otic capsule is due to high levels of secreted osteoprotegerin (OPG) [7, 8], a major negative regulator of osteoclastogenesis and consequent bone resorption. By binding RANKL (receptor activator of NFκB ligand) [9], OPG acts as a decoy receptor and prevents RANKL-RANK interactions and the downstream RANK-mediated nuclear factor kappa B (NFκB) activation that is critical for initiation of osteoclast

differentiation. In *Opg*$^{-/-}$ mice, massive erosion of auditory ossicles and the otic capsule by unchecked osteoclasts leads to compensatory abnormal osteogenesis, causing fixation of the stapes and consequent progressive hearing loss due [10, 11].

In humans, reduced OPG in the otic capsule is associated with otosclerosis [12, 13], a condition characterized by abnormal growth of bone at one or more foci within the middle ear or inner ear that often leads to hearing loss in patients. Otosclerosis develops initially through a first phase of bone resorption by activated osteoclasts and increased vascularization (the otospongiosis phase), followed by new bone deposition from osteoblasts and mineralization (the otosclerosis phase) [13]. The prevalence of otosclerosis is high in Caucasians compared to patients of African descent and higher in women than men [14]. The etiology of otosclerosis is not well understood, but both genetic and environmental factors, including measles virus infection, hormonal changes during pregnancy and middle ear inflammation, have been postulated to contribute. Family linkage analyses and candidate gene association studies have identified several loci associated with otosclerosis, yet none of the otosclerosis causing genes within these regions has been identified so far [15–17]. Nevertheless, mutations in *SERPINF1* or *MEPE* have been recently associated with familial otosclerosis [18, 19]. Given that maintaining OPG level is fundamental to the prevention of bone turnover in the middle and inner ear and the consequent development of otosclerosis, a better understanding of the molecular mechanisms that regulates OPG expression will provide clues regarding the underlying biological basis of the disease.

In this study, we demonstrate a role for the L-type $Ca_V1.2$ voltage-gated calcium channel (VGCC) in the regulation of OPG expression in the middle and inner ear. The $Ca_V1.2$ channel is widely distributed and mediates Ca^{2+} influx into the cell upon membrane depolarization. The entry of Ca^{2+} causes a transient increase of intracellular $[Ca^{2+}]i$, which serves as a second messenger and mediates critical physiological roles in many organs, including cardiac muscle contraction, hormone secretion in endocrine tissues, postsynaptic responses in various 5 neurons, and activation of gene expression paradigms [20]. However, its role in the auditory ossicles and the otic capsule was not previously reported. The $Ca_V1.2$ channel is composed of multiple subunits: α_{1C}, β, and α2δ [21]. The α_{1C} subunit is the ion-conducting pore while the β and α2δ are auxiliary subunits that modulate channel properties [22]. Most studies focused on $Ca_V1.2$ function in excitable cells such as cardiomyocytes and neurons, where frequent and dynamic changes in membrane potential facilitate activation of the voltage-gated channel, with little attention to potential contributions of the channel in non-excitable cells. Studies of Timothy syndrome (TS), a multiorgan disorder caused by *de novo* gain-of-function missense mutations in the α_{1C}-encoding *CACNA1C* gene [23, 24], revealed critical but previously unappreciated roles for $Ca_V1.2$ in many non-excitable cells. We and others demonstrated that $Ca_V1.2$ was expressed in osteoblast progenitors during long bone development and homeostasis [25–27]. Moreover, in an *in vitro* MC3T3-E1 cell and a primary calvaria organ culture system, Ca^{2+} signaling through $Ca_V1.2$ regulated OPG expression [28]. Pharmacological blocking of $Ca_V1.2$ channel activity with nifedipine reduced the level of OPG expression and secretion [28]. Consistent with those findings, we exploited the TS-causing mutant channel ($Ca_V1.2^{TS}$) to increase Ca^{2+} signaling specifically in osteoblasts or their progenitors and observed inhibited osteoclast activity in long bones through upregulated OPG expression and secretion [25].

Given its ability to modulate the OPG/RANKL/RANK pathway, we hypothesized that $Ca_V1.2$ could also affect bone modeling in the ear. Here, we show that increased Ca^{2+} signaling through $Ca_V1.2^{TS}$ expressed in the auditory ossicles and the otic capsule affected bone modeling/remodeling as well as auditory and vestibular function. Defining the role of Ca^{2+} signaling through $Ca_V1.2$ in the physiological regulation of osteoclast formation offers insights into the mechanisms underlying the pathophysiology of otosclerosis and other bony disorders of the ear and provides clues for future explorations of therapeutic strategies or prevention of hearing loss caused by bony structural changes in the middle and inner ear.

2. Materials and Methods

2.1. Experimental mouse models

All animals were handled according to protocols approved by the Institutional Animal Care and Use Committee at Duke University and at Weill Cornell Medical College. *Rosa26-$Ca_V1.2^{TS}$* and *Col2a1-Cre* have been described previously [29–31]. Homozygous *Rosa26-$Ca_V1.2^{TS}$* female mice were crossed with *Col2a1-Cre* males to generate *Col2a1-Cre;$Ca_V1.2^{TS}$* mutant progeny and *Cre*-negative littermate controls [31] with both sexes used in all experiments.

2.2. X-gal staining

X-gal (5-bromo-4-chloro-3-indolyl-β-D-galactopyranoside) staining was performed on whole mount specimens. The auditory ossicles, the inner ear vestibular system and cochlea were fixed in 4% paraformaldehyde on ice for 1 hour, washed three times with 1 × PBS, and stained with X-gal solution (5 mM potassium ferrocyanide, 5 mM potassium ferricyanide, 1 mg/ml X-gal, 2 mM $MgCI_2$, 0.1% sodium deoxycholate, 0.2% IGEPAL CA-630) in the dark for 12 hours at 37 °C.

2.3. μCT analysis of mice

Specimens were fixed in 10% neutral buffered formalin, washed three times with 1 × PBS, and then embedded in 2% agarose gel in a 50 ml centrifuge tube. Images were obtained with a Scanco VivaCT 80 scanner (Scanco Medical AG, Switzerland) set to 55 kVp and 145 μA, voxel size 10.4 μm.

2.4. Histology and TRAP staining

Specimens were fixed in 10% neutral buffered formalin, washed three times with 1 × PBS, then decalcified in 14% EDTA at 4 °C for 2 weeks. Samples were processed for paraffin embedding and then sectioned at 10 μm thickness.

Alcian Blue Hematoxylin /Orange G (ABH/OG) staining and TRAP staining were performed following standard protocols.

2.5. Real-time PCR

The otic capsule surrounding the cochlear part of the control and *Col2a1-Cre;*$Ca_V1.2^{TS}$ mutant mice at 8 weeks of age was carefully dissected, and grinded in a bath of liquid nitrogen using the disposable micro Tissue homogenizer (BioMasher, Japan). Ground samples were collected with 500 µl Trizol (Qiagen) and total RNA was purified using the ZR tissue & Insect RNA MicroPrep kit (Zymo Research, Irvine, CA, USA). qPCR was performed using SYBR green Supermix (Bio-Rad). The primers for *Opg* and *Rankl* and *Gapdh* have been described previously [25]. Gene expression was first normalized to *Gapdh* and then normalized to control samples.

2.6. Auditory Brainstem response (ABR) test

The 6-week old mice were anesthetized with ketamine (125 mg/kg) and xylazine (12.5 mg/kg) via intraperitoneal injection prior to all procedures. Once a suitable plane of anesthesia was reached, the portion of the pinna which obscured the entrance to the tested ear canal was removed. The anesthetized animal was then placed in a sound-isolated, electrically-shielded box on top of a heating pad (40-90-2-05, FHC, Inc.). In conjunction with the heating pad, a rectal probe and DC temperature controller (41-90-8D, FHC, Inc.) were used to maintain the mouse's temperature near 38 °C. Both eyes were moistened with ophthalmic ointment (Puralube®, Dechra Veterinary Products). Needle electrodes (GRD-SAF, The Electrode Store) were subdermally placed behind the pinna of the tested ear (reference electrode), in the scalp between the ears (active electrode), and in the back near the tail (ground electrode). ABRs were evoked by tone bursts of 4, 8, 16, and 32 kHz produced by a closed-field magnetic speaker connected to a power amplifier (MF1 and SA1, Tucker-Davis Technologies). Each 5-ms burst was presented 33.3 times per second with alternating polarity. The onset and offset of each burst was tapered with a squared cosine function. For each frequency, the sound pressure level was lowered from 80 dB SPL in 5–10 dB steps until the threshold was reached. If 80 dB SPL was not enough to elicit a response, higher intensities were produced. The speaker's output was transmitted into the ear through a custom acoustic coupler. The entire sound delivery system was calibrated with a ¼ inch condenser microphone (4939-A-011 and 2690-A-0S1, Brüel & Kjær). The electrical response evoked by the tone bursts and measured by the needle electrodes was amplified 10,000 times and bandpass filtered at 0.3–3 kHz (P55, Astro-Med Inc.). The amplified response was then digitally sampled at 10-µs intervals with a data acquisition device (PCI-6259, National Instruments) controlled by custom software (LabVIEW 2014, National Instruments). The electrical responses to 1,000 bursts were averaged at each intensity level to determine the threshold, which was defined as the lowest level at which any response peak was distinctly and reproducibly present. Visual inspection of the vertically stacked responses facilitated threshold determination.

2.7. Behavioral Testing

Spontaneous activity in an open field arena was monitored with Fusion Open Field Legacy system (Omnitech Electronics Inc., Columbus, OH) over 15 minutes. Mice at 6 weeks of age were singly placed in a 20 × 20 × 40 cm Plexiglas open field arena where activity was monitored by two rows of infrared diodes interfaced to a computer running Fusion 5.3 software. The activity of the animals in the open field were also recorded to digital video from a camera mounted over each test arena using Noldus Media Player (Noldus Information Technologies). The total distance (cm) moved and the circling activity as scored with Fusion software is reported. Circling is defined as the combination of clockwise and counter-clockwise circles performed by the mouse in the open field. In a separate test, balance and coordination were examined using a steady state rotarod at 25 rpm (Medd-Associates, St. Albans, VT). The steady speed was selected on a basis of an accelerated speed (4-40 rpm) given 24 hours prior to the steady speed test. This study showed that the average speed at which the mice fell from an accelerating rotarod was approximately 25 rpm. For the steady speed rotarod test, mice were given four 5-minute trials separated by a 20 min inter-trial interval (ITI). In all cases, trials terminated when the mouse fell from the rod or at 300 seconds. This time (s) was recorded as the latency to fall from the rod.

2.8. Statistics

All statistical analyses were performed using GraphPad Prism 7.0 by two-tailed unpaired Student's *t* tests. Data were presented as mean ± SD or mean ±SEM from n > 3 experiments. Two-sided p values less than 0.05 were considered statically significant. qPCR analyses were performed with > 3 independent RNA isolates and triplicates for each RNA sample. Fold changes were calculated by dividing the value of the mutant mice by the value of the control mice. Increasing or decreasing percentage changes were calculated by dividing the value of difference between the treatment group and control group by the value of the control group and then multiplying 100.

3. Results

3.1. Middle and inner ear appearance in Col2a1-Cre;$Ca_V1.2^{TS}$ mice

To examine whether $Ca_V1.2$ contributes to development of the auditory ossicles and the otic capsule, we tested whether increasing Ca^{2+} signaling specifically through Cav1.2 affected the structure of the ossicles and otic capsule. We employed a $Ca_V1.2^{TS}$ transgenic mouse model, in which $Ca_V1.2^{TS}$ expression was silenced by a floxed upstream stop codon. We activated $Ca_V1.2^{TS}$ mutant channel expression in the bones of ear with *Col2a1-Cre,* which targets the osteochondral progenitors [31]. Targeted *Col2a1-Cre* expression in the auditory ossicles and the otic capsule was confirmed with *Col2a1-Cre;Rosa26-lacZ* reporter mice (Fig. 1). The *Col2a1-Cre* directed *lacZ* expression in the ossicles and otic capsule, detected by prominent β-galactosidase staining that was absent in *Rosa26-lacZ* reporter mice

lacking the *Col2a1-Cre*. We then examined the morphology of the isolated auditory ossicles and the otic capsule from *Col2a1-Cre;*$Ca_V1.2^{TS}$ mutant mice and their *Cre*-negative littermate controls at 6 weeks of age. We found that the auditory ossicles and the otic capsule of $Ca_V1.2^{TS}$-expressing mutant mice were thicker and had more bone mass than those of the control mice, particularly at the malleus handle, the malleus bony membrane, the incus body, the footplate of stapes, the stapedial arch (especially the anterior and posterior crura), and the whole otic capsule (Fig. 2A–D). In *Col2a1-Cre;*$Ca_V1.2^{TS}$ mutant mice, narrowed spaces were observed between the stapedial crura (through which the stapedial artery passes), for the round window and the oval window of the otic capsule. μCT 3-D reconstruction images of the auditory ossicles and the otic capsules confirmed the thicken bones and massive increase of bone mass in the malleus, incus, stapes and the otic capsules of the *Col2a1-Cre;*$Ca_V1.2^{TS}$ mutant mice as well as the narrowed cavities for the stapedial artery and the cochlea (Fig. 2E–H).

Fig. 1. Characterization of *Col2a1-Cre* activity in the auditory ossicles and the otic capsule using the *Rosa26-lacZ* reporter mice.

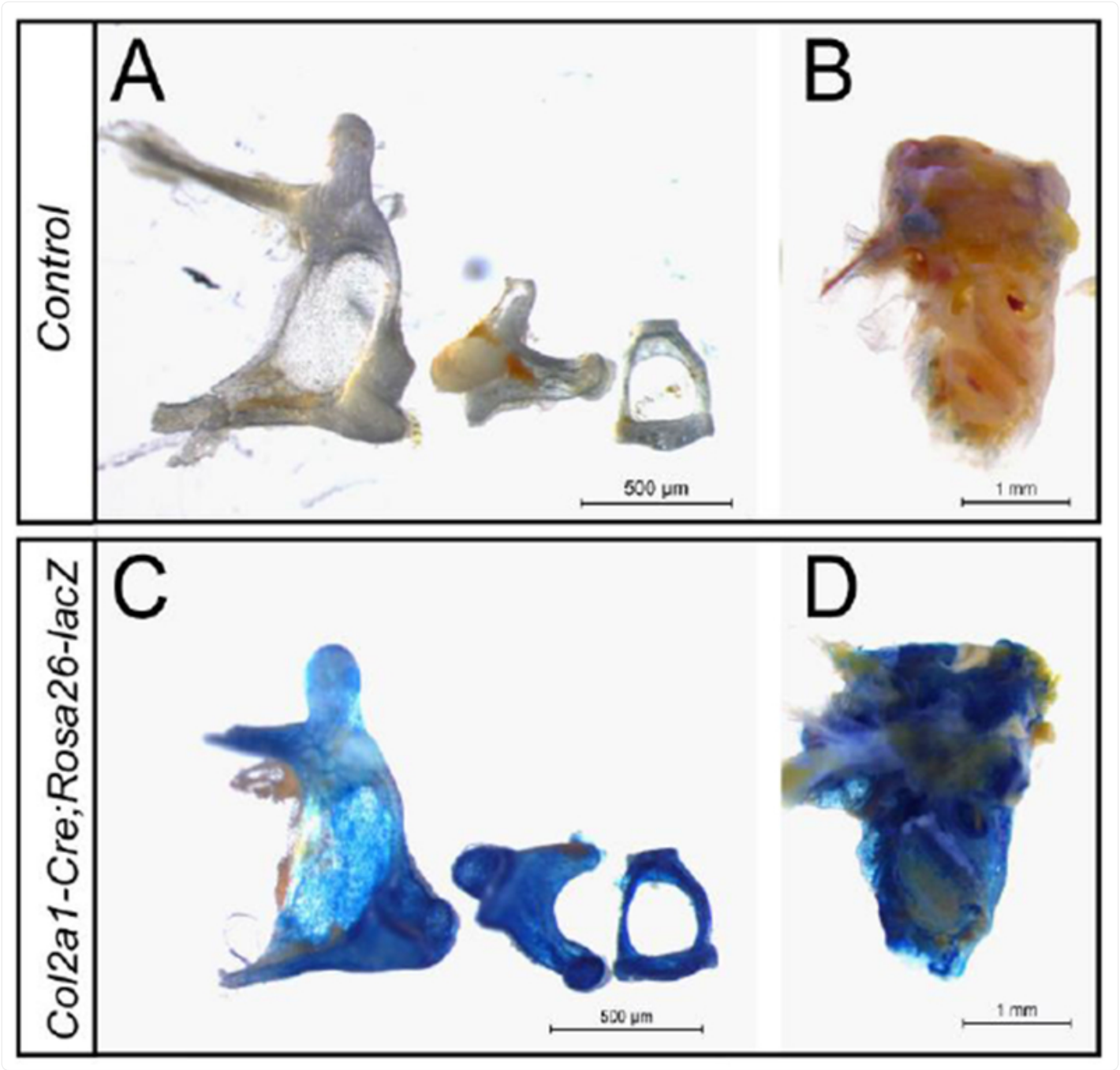

Open in a new tab

Wholemount X-gal staining of the auditory ossicles (malleus, incus, and stapes), the vestibular system and cochlea from *Cre*-negative littermate controls (A and B) and *Col2a1-Cre;Rosa26-lacZ* mice (C and D) at 6 weeks of age.

Fig. 2. Expression of the $Ca_V1.2^{TS}$ mutant channel affects the morphology and increases bone mass of the auditory ossicles and the otic capsule.

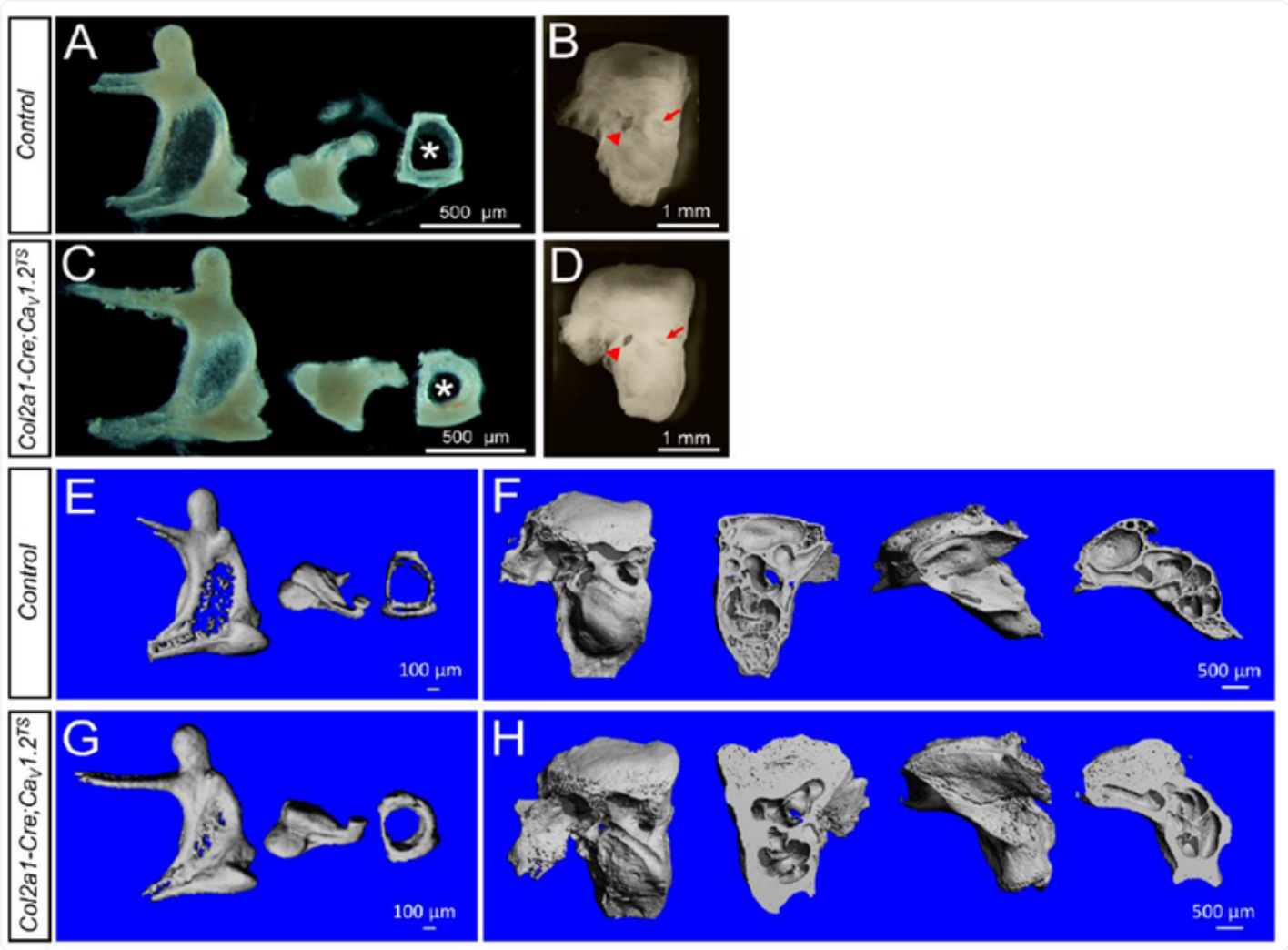

Open in a new tab

A-D, Photomicrographs of the auditory ossicles (malleus, incus, and stapes), vestibular system and cochlea from *Cre*-negative littermate controls (A and B) and *Col2a1-Cre;*$Ca_V1.2^{TS}$ mice (C and D) at 6 weeks of age. Asterisk indicates the space between the stapedial crura (the obturator foramen), where the stapedial artery passes. Arrow heads indicate the oval window and arrows indicate the round window. E-H, µCT 3-D reconstruction of the auditory ossicles, vestibular system and cochlea of *Cre*-negative littermate controls (E and F) and *Col2a1-Cre;*$Ca_V1.2^{TS}$ mice (G and H) at 6 weeks of age.

Histological examination and staining with Alcian Blue Hematoxylin/Orange G (ABH/OG) of the otic capsule showed

that in *Col2a1-Cre;*$Ca_V1.2^{TS}$ mutant mice the original bone marrow region was occupied with excessive bone, while the organ of corti was largely intact (Fig. 3A–F). We also observed extensive Alcian Blue-stained cartilage remnant in the bones of the mutant mice besides the Alcian Blue-stained cartilage remnant of the globuli interossei in the cochlea, suggesting osteoclast defects in the mutant mice. Moreover, the mutant otic capsules lacked sculpting, further indicative of defective osteoclast function.

Fig. 3. Histological analysis of the inner ear of the *Col2a1-Cre;Ca$_V$1.2^{TS}* mice.

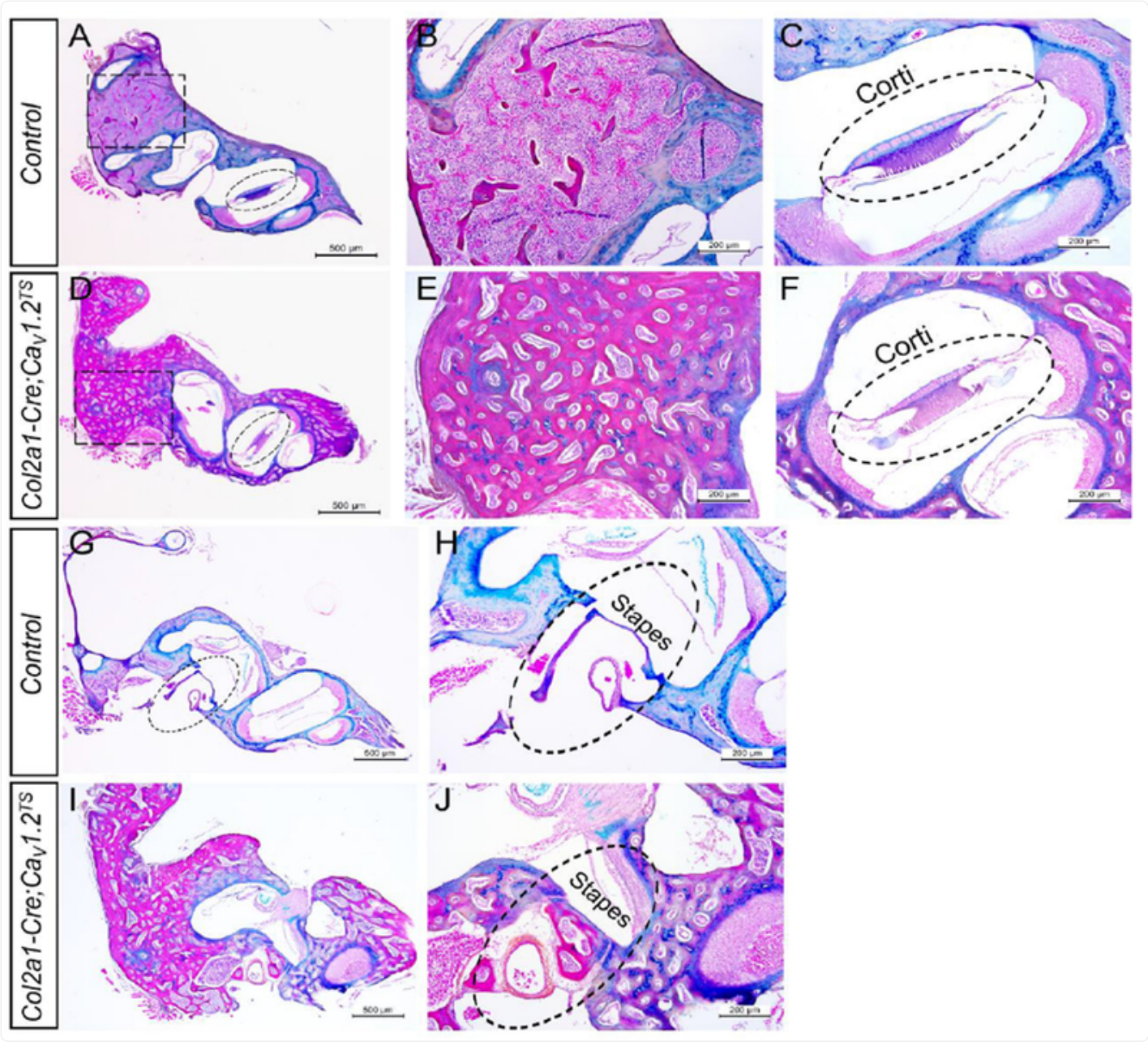

Open in a new tab

A-F, Alcian Blue Hematoxylin/Orange G (ABH/OG) staining of sagittal sections from the inner ear of *Cre*-negative littermate controls (A, with higher magnification in B and C) and *Col2a1-Cre;Ca$_V$1.2^{TS}* mice (D, with higher magnification E and F) at 4 weeks of age, showing excessive bone mass in the vestibular system and cochlea but with little changes in the organ of corti of *Col2a1-Cre;Ca$_V$1.2^{TS}* mice. G-J, ABH/OG staining of the stapedio-vestibular junction of *Cre*-negative controls (G, with higher magnification in H) and *Col2a1-Cre;Ca$_V$1.2^{TS}* mice (I, with higher magnification in J) at 4 weeks of age, showing the stapes footplate was not

fixed but increased bone volume of stapes footplate and vestibule likely limited its movement in *Col2a1-Cre;*$Ca_V1.2^{TS}$ mice.

We histologically examined the stapedio-vestibular joint space in the *Col2a1-Cre;*$Ca_V1.2^{TS}$ mutant and control mice and found that it was not fixed in the $Ca_V1.2^{TS}$-expressing mutant mice (Fig. 3G–J). However, the enlarged bone volume in the stapes footplate and the otic capsule likely limited the stapes movement.

Because the histology indicated defective osteoclast function in the mutant mice, we analyzed the effect of increased Ca^{2+} signaling through $Ca_V1.2^{TS}$ on osteoclasts. We performed tartrate-resistant acid phosphatase (TRAP) staining on histological sections of the otic capsules *Col2a1-Cre;*$Ca_V1.2^{TS}$ mutant mice and littermate controls at 2 weeks of age. Compared to the controls, we observed significantly less TRAP-staining and fewer osteoclasts in the otic capsule of *Col2a1-Cre;*$Ca_V1.2^{TS}$ mutant mice (Fig. 4A–F). We next quantitated the number of TRAP-positive multinucleated osteoclasts and osteoclast area, both of which were normalized to the bone area. The number of osteoclasts per bone area (Oc.N/B.Ar) was decreased by 91% and osteoclast area per bone area (Oc.Ar/B/Ar) decreased by 79% in *Col2a1-Cre;*$Ca_V1.2^{TS}$ mice (Fig. 4G), suggesting that osteoblastic bone resorption of the otic capsule is greatly reduced in *Col2a1-Cre;*$Ca_V1.2^{TS}$ mice during postnatal development. As *Col2a1-Cre* expression is restricted to osteochondral lineage but not to osteoclast progenitors, increased Ca^{2+} signaling through $Ca_V1.2^{TS}$ mutant channel could inhibit osteoclastogenesis via interfering with the OPG/RANKL/RANK pathway in the otic capsule, similar to that we observed in the long bone [25]. We therefore examined *Opg* and *Rankl* mRNA expression in the otic capsule surrounding the cochlea of *Col2a1-Cre;*$Ca_V1.2^{TS}$ mutant mice and their littermate controls. Indeed, RT-qPCR analysis revealed upregulated (~4.4 fold) *Opg* mRNA expression in the otic capsule of *Col2a1-Cre;*$Ca_V1.2^{TS}$ mutant mice compared with that in the control mice but no significant change in *Rankl* mRNA expression, thus resulting in an increase (~2.6 fold) in *Opg/Rankl* mRNA expression ratio in the otic capsule (Fig. 4H). We also detected upregulated mRNA expression of genes for osteoblast differentiation, such as *Alpl, Runx2* and *Sp7* in the otic capsule of *Col2a1-Cre;*$Ca_V1.2^{TS}$ mutant mice (Fig. 4I), suggesting an anabolic effect of $Ca_V1.2^{TS}$ also contributed the increased bone mass in the auditory ossicles and the otic capsule of *Col2a1-Cre;*$Ca_V1.2^{TS}$ mutant mice.

Fig. 4. Decreased osteoclast differentiation and increased osteoblast differentiation in the otic capsule of *Col2a1-Cre;Ca$_V$1.2^{TS}* mice.

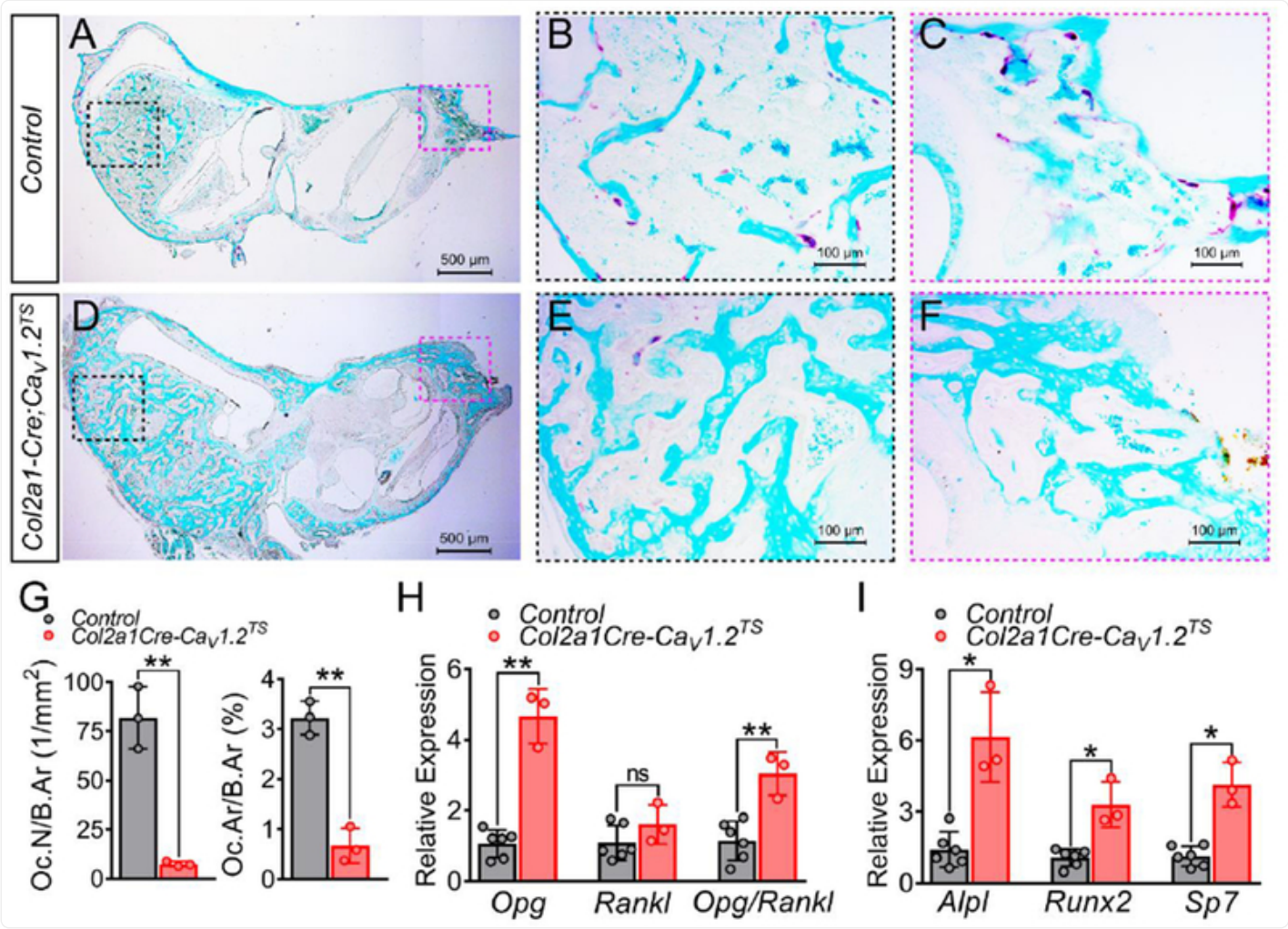

Open in a new tab

A-F, Representative images of TRAP staining counterstained with Fast Green in the otic capsule sections from 2-week-old *Cre*-negative littermate controls (A, with higher magnification in B and C) and *Col2a1-Cre;Ca$_V$1.2^{TS}* mice (D, with higher magnification in E and F). G, Analysis of osteoclast number (Oc.N) and osteoclast area (Oc.Ar) over bone area (B.Ar) of the otic capsule. Bar values are means ± SD, n = 3, ** $p < 0.01$ by 2-tailed unpaired *t* test. H-I, RT-qPCR analysis of mRNA expression of *Opg, Rankl* and *Opg/Rankl* ratio (H) and three osteoblast differentiation markers *Alpl, Runx2* and *Sp7* (I) in the otic capsule surrounding the cochlea of *Cre*-negative controls and *Col2a1-Cre;Ca$_V$1.2^{TS}* mice at 8 weeks of age. $n \geq 3$; Bar values are shown as mean ± SD, ** $p < 0.01$ by 2-tailed unpaired *t* test.

3.2. Col2a 1-Cre;$Ca_V1.2^{TS}$ mice are hearing impaired

To assess whether the morphological changes in the auditory ossicles and the otic capsule in the *Col2a1-Cre;$Ca_V1.2^{TS}$* mutant mice impaired auditory function, we tested the auditory brainstem response (ABR) in both *Col2a1-Cre;$Ca_V1.2^{TS}$* mutant mice and their littermate controls at 6 weeks of age. Representative responses from control (Fig. 5A) and *$Ca_V1.2^{TS}$*-expressing mutant mice (Fig. 5B) to decreasing stimulus intensities at 8 kHz showed differences in sensitivity and latency between the two genotypes. Compared to the control mice, the *Col2a1-Cre;$Ca_V1.2^{TS}$* mutant mice had no response to intensities below 85 dB SPL at 8 kHz and below 75 dB at 16 kHz (Fig. 5C and 5D). The mutant mice also showed delays for even stronger stimulus intensities (Fig. 5C and 5D). Furthermore, the hearing threshold of the *Col2a1-Cre;$Ca_V1.2^{TS}$* mutant mice was significantly higher (lower sensitivity) than that of the control mice in the 4 to 16 kHz region, while we found no significant difference in threshold between two genotypes at 32 kHz (Fig. 5E). That the hearing loss in *Col2a1-Cre;$Ca_V1.2^{TS}$* mutant mice is spared only in the high-frequency range is consistent with a conductive hearing loss mechanism, in which sounds fail to be transferred via the ossicular chain in the middle ear to the cochlea.

Fig. 5. Auditory Brainstem Response testing shows hearing loss in *Col2a1-Cre;*$Ca_V1.2^{TS}$ mice.

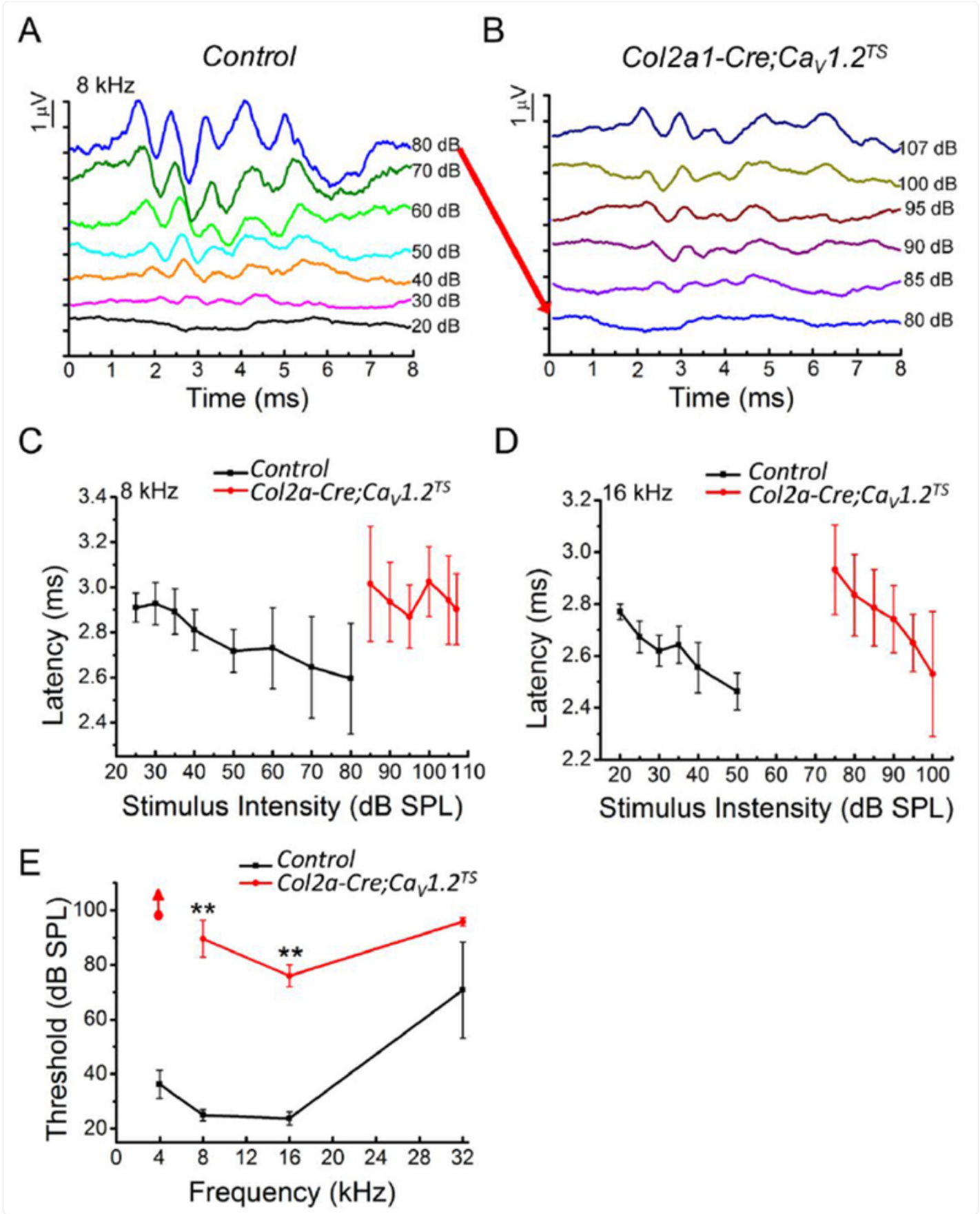

Open in a new tab

A and B, Representative latency responses to different stimuli were compared between *Cre*-negative littermate controls (A) and *Col2a1-Cre;*$Ca_V1.2^{TS}$ mice (B) at 8 kHz. C and D, The latency-intensity function curves were recorded at 8 kHz (C) and 16 kHz (D) with the littermate controls at the left part of the curve (black) and *Col2a1-Cre;*$Ca_V1.2^{TS}$ mice at the right part of the curve (red). E, The threshold curves were significantly different between the littermate controls and *Col2a1-Cre;*$Ca_V1.2^{TS}$ mice at 4, 8 and 16 kHz frequencies (red arrow: no hearing response in *Col2a1-Cre;*$Ca_V1.2^{TS}$ mice was detected at 98 dB at 4 kHz). n = 4 for controls; n = 5 for *Col2a1-Cre;*$Ca_V1.2^{TS}$ mice; Data are shown as mean ± SEM, ** $p < 0.01$ by 2-tailed unpaired t test.

3.3. Col2a1Cre;$Ca_V1.2^{TS}$ mice show impaired vestibular function

Otosclerosis patients sometimes experience vestibular symptoms in addition to hearing loss. Because of the observed morphological changes in the vestibular system in *Col2a1-Cre;*$Ca_V1.2^{TS}$ mutant mice, we also examined their motor activities in an open field arena. The $Ca_V1.2^{TS}$-expressing mutants were significantly more active compared to the control animals (mean distance moved ± SEM: Control = 1160 cm ± 125; *Col2a1-Cre;*$Ca_V1.2^{TS}$ = 4,362 cm ± 529; $p < 0.01$). Additionally, we found that the $Ca_V1.2^{TS}$-expressing mice exhibited frequent and random circling behavior in both the clockwise and counter clockwise directions (Fig. 6A and Supplementary Video), which lasted up to 8 seconds, indicating defects in vestibular function. We also evaluated body balance and coordination with the rotarod test. When accelerating the rotarod from 4 to 40 rpm, the *Col2aCre-*$Ca_V1.2^{TS}$ mutant mice fell off earlier, at an average speed of 25 rpm (Fig. 6B), and showed a significant decrease in the latency to fall (Fig. 6C). Furthermore, on the steady state rotarod at 25 rpm, the latency to fall was decreased across all four trials for *Col2a1-Cre;*$Ca_V1.2^{TS}$ mutant mice compared to that for the controls (Fig. 6D). Taken together, the behavior studies showed that *Col2a1-Cre;*$Ca_V1.2^{TS}$ mutant mice have a defect in vestibular function, affecting balance and coordination.

Fig. 6. Deficits of body balance in *Col2a1-Cre;Ca$_V$1.2^{TS}* mice.

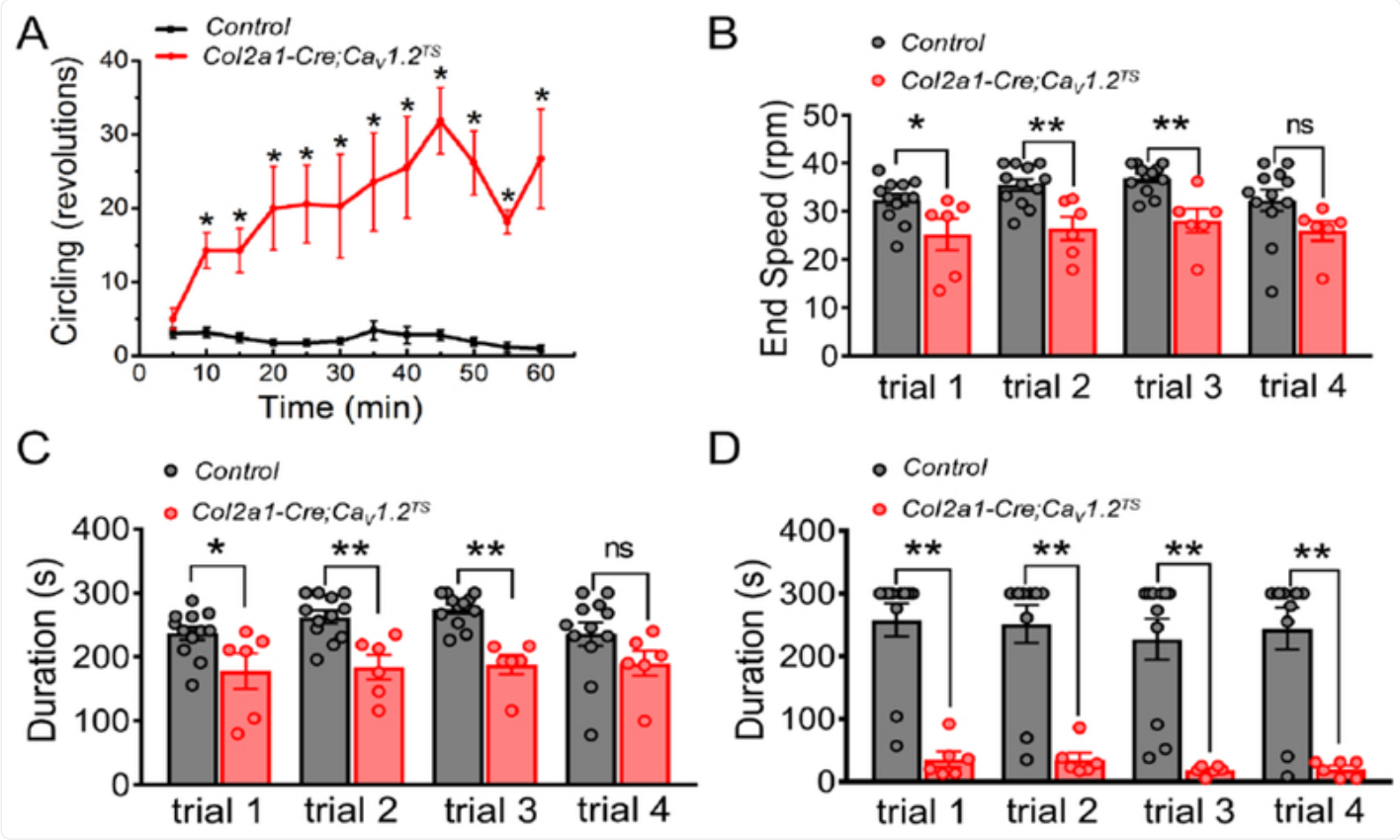

Open in a new tab

A, *Col2a1-Cre;Ca$_V$1.2^{TS}* mice displayed circling behavior in the open field test without preference for a particular direction, while *Cre*-negative littermate controls remained quiet most of the time. B and C, the end speed (B) and the duration (C, the latency to fall) on accelerating rotarod (from 4 to 40 rpm) for *Col2a1-Cre;Ca$_V$1.2^{TS}* mice over all four trials compared with *Cre*-negative littermate controls. D, the duration on the steady state rotarod test (25 rpm) for *Col2a1-Cre;Ca$_V$1.2^{TS}* mice over all four trials compared with *Cre*-negative littermate controls. n = 11 for controls; n = 6 for *Col2a1-Cre;Ca$_V$1.2^{TS}* mice; Data are shown as mean ± SEM, * $p < 0.05$; ** $p<0.01$. Statistical analysis was performed by 2-tailed unpaired t test.

Discussion

Our data demonstrate that Ca^{2+} influx through $Ca_V1.2$ regulates development of the auditory ossicles and otic capsule. Moreover, excessive Ca^{2+} influx through TS-causing mutant $Ca_V1.2$ channel causes deficits in both hearing and body balance. The abnormal bone growth of the auditory ossicles and the otic capsule in *Col2a1-Cre;Ca$_V$1.2^{TS}* mice is likely

due to both increased bone formation and decreased bone resorption, similar to the dual effect of the $Ca_V1.2^{TS}$ mutant channel on long bones that we previously demonstrated [25].

Although osteoclastogenesis is normally suppressed in the ossicles and the auditory otic capsule because of a locally high level of OPG, osteoclast function is still required to sculpt these bones during development. Absence of osteoclastic bone resorption in *Rankl*$^{-/-}$, *Fos*$^{-/-}$ and *Csf1*$^{op/op}$ mice significantly affected these bones morphologically and functionally [4]. Expression of the gain-of-function $Ca_V1.2^{TS}$ mutant channel in our *Col2a1-Cre;*$Ca_V1.2^{TS}$ mice affected the overall morphology of the auditory ossicles and the otic capsule, which display reduced sculpting (see the stapedial crura) and an osteopetrotic phenotype that are strikingly similar to those seen in *Rankl*$^{-/-}$, *Fos*$^{-/-}$ and *Csf1*$^{op/op}$ osteoclastic defect mice [4], suggesting that the anticatabolic effect of increased Ca^{2+} signaling through $Ca_V1.2^{TS}$ contributed to the morphological changes in theses bones. While this is the first demonstration, to our knowledge, showing that modulating Ca^{2+} signal via $Ca_V1.2$ in the auditory ossicles and the otic capsule regulates osteoclastogenesis and bone modeling/remodeling in the middle and inner ear, our data are consistent with previous observations from others and us that $Ca_V1.2$ regulates OPG expression and secretion from osteoblasts [25, 28]. That expression of the $Ca_V1.2^{TS}$ mutant channel in our model was driven by *Col2a1-Cre,* which restricts expression to chondrocytes and osteoblast precursors but not in osteoclasts or their progenitors [31], adds further support to our hypothesis that the anticatabolic responses by altered $Ca_V1.2$ activity is mediated by upregulated OPG expression and secretion in bones of the ear. Our data showing increased *Opg* mRNA expression in the otic capsule surrounding the cochlea in *Col2a1-Cre;*$Ca_V1.2^{TS}$ mice further supports this hypothesis.

Moreover, since the $Ca_V1.2^{TS}$ transgene expression is driven by *Col2a1-Cre,* the hearing and vestibular defects we observed can be attributed to the abnormal bone, and not to mutant channel expression in the hair cells of the cochlea and vestibular system or downstream nerves, in which *Col2a1-Cre* is not active. Consistent with that hypothesis, the organ of Corti is grossly intact in *Col2a1-Cre;*$Ca_V1.2^{TS}$ mice (Fig. 4). However, as aberrant bone remodeling progresses in *Col2a1-Cre;*$Ca_V1.2^{TS}$ mice, it is also possible that the increased bone formation of the auditory ossicles and the otic capsule and narrowed cavities in the bony labyrinth of the otic capsule could impair neuronal function and contribute to the circling behavior and hearing impairment. Thus, eventually both bone structure and neuronal dysfunction may contribute to the observed defects in hearing and vestibular function.

Our results may also provide insight into the utility of sodium fluoride (NaF) as a treatment option to prevent hearing deterioration in patients with otosclerosis [32] and the reported association between clinical otosclerosis and low fluoride content in the drinking water [33–35]. Although this correlation has not been consistently observed, and the underlying mechanism of effect of fluoride on otosclerosis has not been sufficiently established, it is intriguing that fluoride, which plays an important role in both bone formation and homeostasis of bone mineral metabolism [36], has been shown to affect Ca^{2+} homeostasis in many types of cells such as in proximal tubules [37, 38], fibroblasts [39], cardiomyocytes [40], as well as osteoblasts [41]. Further, expression of $Ca_V1.2$ was stimulated by low-dose fluoride, inhibited by high-dose fluoride [42], and fluoride can stimulate cardiac L-type Ca^{2+} channel activity by increasing

channel open probability or the duration of channel opening in a dose-dependent manner [40]. Our finding of upregulated OPG mRNA expression and OPG mediated-osteoclastogenesis inhibition in the otic capsule upon increased Ca^{2+} signaling via $Ca_V1.2$ may add a new dimension to the effectiveness of sodium fluoride treating patients with osteosclerosis.

Supplementary Material

1

Download video file (2.7MB, mp4)

Highlights.

1. The voltage-gated $Ca_V1.2$ Ca^{2+} channel regulates (re)modeling of ear auditory ossicles and otic capsule.
2. Perturbed $Ca_V1.2$ function affects OPG levels and consequent osteoclastic activity in ear bones.
3. These data identify a potential role for Ca^{2+} signaling through $Ca_V1.2$ in otosclerosis.

Acknowledgements

We thank for Dr. A. James Hudspeth (Laboratory of Sensory Neuroscience at The Rockefeller University) for providing the setup and space for the ABR hearing test, Dr. Willian C. Wetsel (Mouse Behavioral and Neuroendocrine Core Facility at Duke University) for his assistance in mouse behavior experimental design and Dr. Marja Hurley (Department of Medicine, University of Connecticut Health Center) for her helpful suggestions.

Funding source

This work was supported by a Harrington Discovery Institute / Harrington Scholar-Innovator Grant, the National Institutes of Health [R01HD090132 to G.S.P. and R01AR071722 to M.J.H.].

Footnotes

Conflicts of interest

All authors have nothing to disclose.

References

1. Frolenkov GI, et al. , Genetic insights into the morphogenesis of inner ear hair cells. Nat Rev Genet, 2004. 5(7): p. 489–98. [DOI] [PubMed] [Google Scholar]

2. Mallo M, Formation of the middle ear: recent progress on the developmental and molecular mechanisms. Dev Biol, 2001. 231(2): p. 410–9. [DOI] [PubMed] [Google Scholar]

3. Zhang Z, et al. , Malleal processus brevis is dispensable for normal hearing in mice. Dev Dyn, 2003. 227(1): p. 69–77. [DOI] [PubMed] [Google Scholar]

4. Kanzaki S, et al. , Impaired vibration of auditory ossicles in osteopetrotic mice. Am J Pathol, 2011. 178(3): p. 1270–8. [DOI] [PMC free article] [PubMed] [Google Scholar]

5. Frisch T, et al. , Volume-referent bone turnover estimated from the interlabel area fraction after sequential labeling. Bone, 1998. 22(6): p. 677–82. [DOI] [PubMed] [Google Scholar]

6. Frisch T, et al. , Estimation of volume referent bone turnover in the otic capsule after sequential point labeling. Ann Otol Rhinol Laryngol, 2000. 109(1): p. 33–9. [DOI] [PubMed] [Google Scholar]

7. Zehnder AF, et al. , Osteoprotegerin in the inner ear may inhibit bone remodeling in the otic capsule. Laryngoscope, 2005. 115(1): p. 172–7. [DOI] [PubMed] [Google Scholar]

8. Stankovic KM, et al. , Differences in gene expression between the otic capsule and other bones. Hear Res, 2010. 265(1-2): p. 83–9. [DOI] [PMC free article] [PubMed] [Google Scholar]

9. Kearns AE, Khosla S, and Kostenuik PJ, Receptor activator of nuclear factor kappaB ligand and osteoprotegerin regulation of bone remodeling in health and disease. Endocr Rev, 2008. 29(2): p. 155–92. [DOI] [PMC free article] [PubMed] [Google Scholar]

10. Kanzaki S, et al. , Resorption of auditory ossicles and hearing loss in mice lacking osteoprotegerin. Bone, 2006. 39(2): p. 414–9. [DOI] [PubMed] [Google Scholar]

11. Zehnder AF, et al. , Osteoprotegrin knockout mice demonstrate abnormal remodeling of the otic capsule and progressive hearing loss. Laryngoscope, 2006. 116(2): p. 201–6. [DOI] [PMC free article] [PubMed] [Google Scholar]

12. Karosi T, et al. , Detection of osteoprotegerin and TNF-alpha mRNA in ankylotic Stapes footplates in connection with measles virus positivity. Laryngoscope, 2006. 116(8): p. 1427–33. [DOI] [PubMed] [Google Scholar]

13. Mansour S, et al. , Middle Ear Diseases. 2018. [Google Scholar]

14. Thys M and Van Camp G, Genetics of otosclerosis. Otol Neurotol, 2009. 30(8): p. 1021–32. [DOI] [PubMed] [Google Scholar]

15. Babcock TA and Liu XZ, Otosclerosis: From Genetics to Molecular Biology. Otolaryngol Clin North Am, 2018. 51(2): p. 305–318. [DOI] [PubMed] [Google Scholar]

16. Rudic M, et al. , The pathophysiology of otosclerosis: Review of current research. Hear Res, 2015. 330(Pt A): p. 51–6. [DOI] [PubMed] [Google Scholar]

17. Ealy M and Smith RJ, The genetics of otosclerosis. Hear Res, 2010. 266(1-2): p. 70–4. [DOI] [PubMed] [Google Scholar]

18. Ziff JL, et al. , Mutations and altered expression of SERPINF1 in patients with familial otosclerosis. Hum Mol Genet, 2016. 25(12): p. 2393–2403. [DOI] [PMC free article] [PubMed] [Google Scholar]

19. Schrauwen I, et al. , Variants affecting diverse domains of MEPE are associated with two distinct bone disorders, a craniofacial bone defect and otosclerosis. Genet Med, 2018. [DOI] [PubMed] [Google Scholar]

20. Catterall WA, Regulation of Cardiac Calcium Channels in the Fight-or-Flight Response. Curr Mol Pharmacol, 2015. 8(1): p. 12–21. [DOI] [PMC free article] [PubMed] [Google Scholar]

21. Catterall WA, Structure and regulation of voltage-gated Ca2+ channels. Annu Rev Cell Dev Biol, 2000. 16: p. 521–55. [DOI] [PubMed] [Google Scholar]

22. Serysheva II, et al. , Structure of the voltage-gated L-type Ca2+ channel by electron cryomicroscopy. Proc Natl Acad Sci U S A, 2002. 99(16): p. 10370–5. [DOI] [PMC free article] [PubMed] [Google Scholar]

23. Splawski I, et al. , Ca(V)1.2 calcium channel dysfunction causes a multisystem disorder including

arrhythmia and autism. Cell, 2004. 119(1): p. 19–31. [DOI] [PubMed] [Google Scholar]

24. Splawski I, et al. , Severe arrhythmia disorder caused by cardiac L-type calcium channel mutations. Proc Natl Acad Sci U S A, 2005. 102(23): p. 8089–96; discussion 8086–8. [DOI] [PMC free article] [PubMed] [Google Scholar]

25. Cao C, et al. , Increased Ca2+ signaling through CaV1.2 promotes bone formation and prevents estrogen deficiency-induced bone loss. JCI Insight, 2017. 2(22). [DOI] [PMC free article] [PubMed] [Google Scholar]

26. Shao Y, Alicknavitch M, and Farach-Carson MC, Expression of voltage sensitive calcium channel (VSCC) L-type Cav1.2 (alpha1C) and T-type Cav3.2 (alpha1H) subunits during mouse bone development. Dev Dyn, 2005. 234(1): p. 54–62. [DOI] [PubMed] [Google Scholar]

27. Wang XT, et al. , Cardiac L-type calcium channel alpha 1-subunit is increased by cyclic adenosine monophosphate: messenger RNA and protein expression in intact bone. J Bone Miner Res, 2000. 15(7): p. 1275–85. [DOI] [PubMed] [Google Scholar]

28. Bergh JJ, Xu Y, and Farach-Carson MC, Osteoprotegerin expression and secretion are regulated by calcium influx through the L-type voltage-sensitive calcium channel. Endocrinology, 2004. 145(1): p. 426–36. [DOI] [PubMed] [Google Scholar]

29. Pasca SP, et al. , Using iPSC-derived neurons to uncover cellular phenotypes associated with Timothy syndrome. Nat Med, 2011. 17(12): p. 1657–62. [DOI] [PMC free article] [PubMed] [Google Scholar]

30. Ramachandran KV, et al. , Calcium influx through L-type CaV1.2 Ca2+ channels regulates mandibular development. J Clin Invest, 2013. 123(4): p. 1638–46. [DOI] [PMC free article] [PubMed] [Google Scholar]

31. Ovchinnikov DA, et al. , Col2a1-directed expression of Cre recombinase in differentiating chondrocytes in transgenic mice. Genesis, 2000. 26(2): p. 145–6. [PubMed] [Google Scholar]

32. Causse JR, et al. , The enzymatic mechanism of the otospongiotic disease and NaF action on the enzymatic balance. Am J Otol, 1982. 3(4): p. 297–314. [PubMed] [Google Scholar]

33. Daniel HJ 3rd, Stapedial otosclerosis and fluorine in the drinking water. Arch Otolaryngol, 1969. 90(5): p. 585–9. [DOI] [PubMed] [Google Scholar]

34. Vartiainen E and Vartiainen T, Effect of drinking water fluoridation on the prevalence of otosclerosis. J Laryngol Otol, 1997. 111(1): p. 20–2. [DOI] [PubMed] [Google Scholar]

35. Vartiainen E and Vartiainen J, The effect of drinking water fluoridation on the natural course of hearing in

patients with otosclerosis. Acta Otolaryngol, 1996. 116(5): p. 747–50. [DOI] [PubMed] [Google Scholar]

36. Mousny M, et al. , The genetic influence on bone susceptibility to fluoride. Bone, 2006. 39(6): p. 1283–9. [DOI] [PubMed] [Google Scholar]

37. Xu H, et al. , Effects of fluoride on the intracellular free Ca2+ and Ca2+-ATPase of kidney. Biol Trace Elem Res, 2007. 116(3): p. 279–88. [DOI] [PubMed] [Google Scholar]

38. Dominguez JH, et al. , Fluoride mobilizes intracellular calcium and promotes Ca2+ influx in rat proximal tubules. Am J Physiol, 1991. 261(2 Pt 2): p. F318–27. [DOI] [PubMed] [Google Scholar]

39. Kawase T, Ishikawa I, and Suzuki A, The calcium-mobilizing action of low concentrations of sodium fluoride in single fibroblasts. Life Sci, 1988. 42(12): p. 1253–7. [DOI] [PubMed] [Google Scholar]

40. Ono K and Arita M, Mechanism of fluoride action on the L-type calcium channel in cardiac ventricular myocytes. Cell Calcium, 1999. 26(1-2): p. 37–47. [DOI] [PubMed] [Google Scholar]

41. Zerwekh JE, et al. , Fluoride rapidly and transiently raises intracellular calcium in human osteoblasts. J Bone Miner Res, 1990. 5 Suppl 1: p. S131–6. [DOI] [PubMed] [Google Scholar]

42. Duan XQ, et al. , Fluoride affects calcium homeostasis and osteogenic transcription factor expressions through L-type calcium channels in osteoblast cell line. Biol Trace Elem Res, 2014. 162(1-3): p. 219–26. [DOI] [PubMed] [Google Scholar]

Associated Data

This section collects any data citations, data availability statements, or supplementary materials included in this article.

Supplementary Materials

1

Download video file (2.7MB, mp4)